Russian Journal of Earth Sciences

Numerical Simulation of Tsunami During the Earthquake in the Philippines 02.12.2023

R. Mazova[1], K. Polyakov[1], and A. Kurkin[1,2,*]

[1]Nizhny Novgorod State Technical University n.a. R. E. Alekseev, Nizhny Novgorod, Russia
[2]V. I. Il'ichev Pacific Oceanological Institute Far Eastern Branch Russian Academy of Sciences, Vladivostok, Russia
* **Correspondence to:** Andrey Kurkin, aakurkin@gmail.com

Abstract: In this paper numerical simulation of tsunami waves is carried out using data from the earthquake off the coast of Mindanao Island in the Philippine Sea on 23 December 2023 in the western part of the Pacific Ocean. The paper considers two scenarios of seismic source localization with different dynamics of the Earth's crust displacement in the seismic source region during the earthquake process. Consideration of two scenarios with different location of keyboard blocks, into which the earthquake source is segmented, allows one to study the influence of source geometry on the characteristics of generated tsunami waves. In the course of simulation, during dynamic displacement of keyboard blocks in the earthquake source, tsunami source formation, tsunami waves and their propagation in the Pacific Ocean water area take place. The wave characteristics of the process along the mainland and island zones in the considered water area were obtained. The results of simulation for the two scenarios are compared with observational data, which makes it possible to identify which type of block arrangement provides better similarity with the recorded tsunami characteristics and, therefore, better describes the real dynamics of the earthquake source.

Keywords: earthquake and tsunami in the Philippines 02.12.2023, earthquake sources, tsunami source, tsunami waves, numerical simulation, tsunami wave characteristics.

Citation: Mazova, R., K. Polyakov, and A. Kurkin (2024), Numerical Simulation of Tsunami During the Earthquake in the Philippines 02.12.2023, *Russian Journal of Earth Sciences*, 24, ES5004, EDN: MWVWQN, https://doi.org/10.2205/2024es000949

1. Introduction

On 23 December 2023 at 14:37 local time (UTC+8) an earthquake with magnitude $M = 7.6$ has happened off the coast of Mindanao Island, Philippines. The epicenter of the earthquake was located in the Sulawesi Sea, about 130 km southeast of Davao City, at a depth of 40 km [*NOAA*, 2023; *USGS*, 2023; *Wikipedia*, 2024a,b]. The earthquake generated a tsunami that propagated in the Pacific Ocean. The first tsunami waves reached the coast of Mindanao Island within minutes after the earthquake. Wave heights in some coastal areas reached 3–5 meters, resulting in significant damage and loss of life [*NOAA*, 2023; *USGS*, 2023; *Wikipedia*, 2024a,b]. The tsunami continued to propagate in the Pacific Ocean, reaching the shores of other islands in the Philippine archipelago, as well as Indonesia and Palau. A few hours later, the tsunami waves reached the shores of the Japanese Islands. Although the height of the waves off the coast of Japan was much smaller than in the Philippines (about 0.5 meters), they still caused some damage and required evacuation of the population from the coastal areas. Figure 1 presents data on aftershocks of the earthquake, their localization and intensity; the color of the circle corresponds to the intensity of the shock: green color corresponds to magnitude 4, yellow to magnitude 5 and minor orange circles correspond to magnitude 6, red circle with the number 7 corresponds to the epicenter of the earthquake to a magnitude 7.6 [*Wikipedia*, 2024b].

After the powerful main shock, with magnitude $M = 7.6$, seismic activity in the region continued to manifest itself with high intensity: in the next 24 hours no less than 39 significant aftershocks were registered, each of which had a magnitude of 5.6 or higher, which in itself is a significant seismic event.

Research Article

Received: 30 July 2024
Accepted: 5 November 2024
Published: 28 November 2024

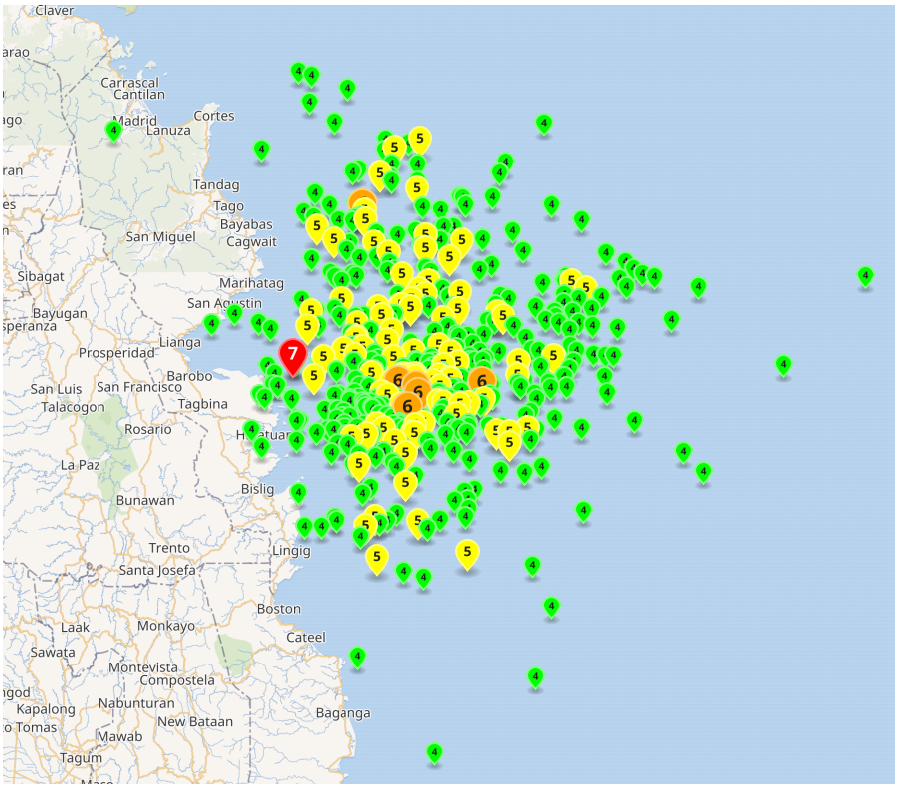

Figure 1. Epicenter and aftershocks of the earthquake 23 December 2023. Numbers on colored circles indicate magnitudes of aftershocks; the color of the circle corresponds to the intensity of the shock; red circle with the number 7 corresponds to the epicenter of the earthquake [*Wikipedia*, 2024b].

2. Problem Statement

2.1. Geographical and Bathymetric Characteristics of the Water Area Under Consideration

The paper considers the Pacific Ocean water area from the earthquake localization point off the coast of Mindanao Island, Philippines, to the coast of the Japanese Islands (Figure 2). Mindanao Island is the second largest island of the Philippine archipelago and is located in its southern part. The earthquake with magnitude 7.6 has happened near the coast, about 19 km to the North-West from Hinatuan city. From the earthquake site, the tsunami propagated east and northeast across the Philippine Sea, which is part of the Pacific Ocean. The Philippine Sea is bounded by the Philippine Islands to the west, the Japanese Islands to the north, the Mariana Islands to the east and the Caroline Islands to the south.

The bathymetry of the Philippine Sea is characterized by the presence of several major underwater geographical features. In the central part of the sea lies the Philippine Plate, which is a section of oceanic crust with depths ranging from 4000 to 6000 meters. To the east, the Philippine Sea is bounded by the Mariana Trench, which is one of the deepest places in the world's oceans with a maximum recorded depth of 11034 meters. To the south, the sea is bounded by a shallower area including the Carolina Plateau and the islands of Yap and Palau with depths ranging from 1000 to 4000 meters. Further north and northeast, the Philippine Sea passes into the Pacific Ocean waters surrounding the Japanese Islands. The Izu-Bonin and Japan Trough with depths up to 8000–9000 meters, as well as a number of underwater ridges and uplands, such as the Kyushu-Palau Ridge, Ogasawara Uplands and Min-Daito Uplands with depths from 2000 to 4000 meters. Directly off the coast of the Japanese Islands, the depths decrease to 500–1000 meters on the shelf and 0–500 meters in the coastal zone [*NOAA*, 2023; *USGS*, 2023; *Wikipedia*, 2024a,b].

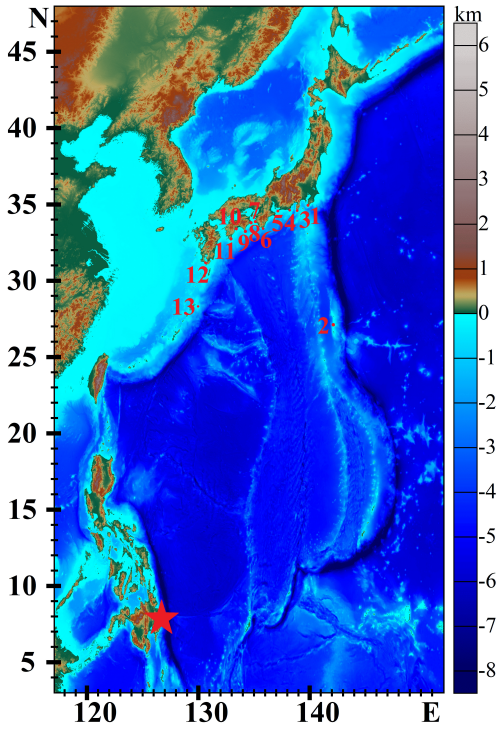

Figure 2. Estimated water area from the Philippine Islands to the Japanese Islands; red asterisk marks epicenter of the earthquake.

Thus, the study area is characterized by a complex and heterogeneous bathymetry, including both deep-sea trench and troughs and underwater ridges, uplands and relatively shallow shelves. These features of the seafloor topography have a significant impact on tsunami wave propagation.

2.2. Seismic Process Parameters and Initial Modeling Conditions

To model and analyze the seismic tsunami caused by this earthquake, the main parameters of the seismic process were determined and the initial conditions of the model were set. To simulate the dynamics of the earthquake source, a keyboard model of tsunamigenic earthquakes [*Lobkovsky and Baranov*, 1984] is used, in which the Earth's crustal rupture region is represented as sequentially moving keyboard blocks. Each block has its own motion parameters such as displacement height, motion onset time and motion duration. Due to the smallness of the horizontal displacement compared to the vertical displacement [*Lobkovsky and Baranov*, 1984], in this model only the vertical displacements of the keyboard blocks was considered. The use of the keyboard-block model allows one to reproduce in detail the dynamics of the earthquake source, including the sequential involvement of different rupture sections in the displacement process and the associated changes in tsunami wave generation. The parameters of block motion are selected in such a way as to ensure that the model results are consistent with available data on the intensity and timing of aftershocks, observational data, including seismic records and recorded tsunami wave characteristics.

Two scenarios with different block locations relative to the coastline of Mindanao Island are considered in this paper:

Scenario 1: 16 blocks forming the origin of the earthquake are located across the coastline.

Scenario 2: 18 blocks forming the earthquake source are located along the fault line. The location of the origin for Scenario 2 is more consistent with the geodynamics of the seismic process in the subduction zone. However, Scenario 1 allows to include the largest number of aftershocks for this earthquake in the zone of the considered source.

2.3. Modeling of Earthquake Source

Table 1 presents data on aftershocks of the earthquake for the first 24 hours, their localization and intensity. After the powerful main shock with magnitude $M = 7.6$ seismic activity in the region continued with high intensity: In the next 24 hours more than 39 significant aftershocks were registered, each of them having magnitude 5.6 or higher, which in itself is a significant seismic event.

Figure 3 shows a part of the considered water area with epicenter and aftershocks given in Table 1 for the first 24 hours after the earthquake. Magnitude values for each aftershock and numbering of sequence of their occurrence are marked on the picture. The color of the circle in the picture and its magnitude corresponds to the intensity of the aftershock.

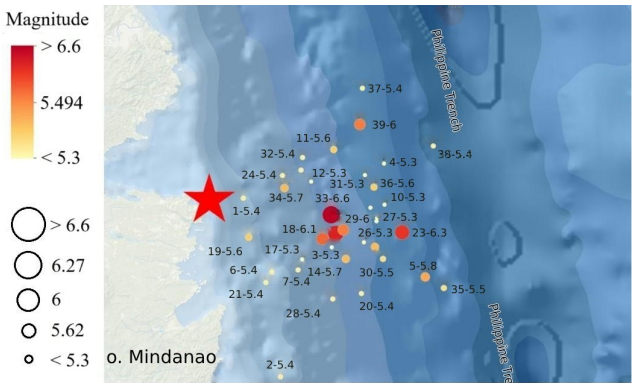

Figure 3. Epicenter and aftershocks of the earthquake in Philippines 02.12.2023 for the first 24 hours after the event. Red star corresponds to epicenter of this earthquake [*Wikipedia*, 2024b].

Figure 4 shows a schematic representation of the source for Scenario 1. The seismic source dimensions were estimated using the Wells formulae [*Wells and Coppersmith*, 1994].

For the first Scenario the earthquake origin is located across the crustal fault zone. Based on the data of Table 1 and Figures 3 and 4, the earthquake origin is constructed, in which the seismic origin is formed from a set of 16 separate blocks (Figure 5). Each block has its own motion characteristics corresponding to the maximum magnitude of aftershock with localization in this block, such as time of displacement onset, displacement height and duration of motion.

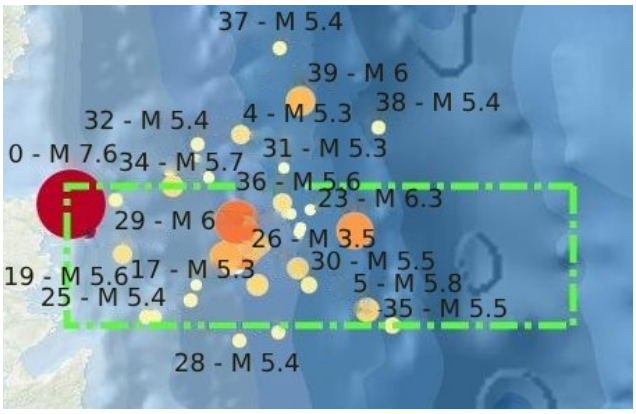

Figure 4. Schematic localization of earthquake origin in Philippines 02.12.2023. colored circles correspond to aftershocks, with marked on them aftershock magnitudes and sequence of aftershocks appearance.

Table 2 shows the data used to model the kinematics of block motion: the coordinates of the corner points, the time of block motion start, the time of block motion, and the height of block lift. The generation of tsunami waves is caused by the displacement of

Table 1. Data on earthquake aftershocks for the first 24 hours, their localizations and intensity [*Wikipedia*, 2024b]

No.	Magnitude	Localization	Times	Coordinates
1	5.4	25 km NE of Hinatuan, Philippines	02 2023 14:44:03	8.5324, 126.5047
2	5.4	18 km ENE of Santa Maria, Philippines	02 2023 14:44:36	8.0495, 126.6059
3	5.3	43 km NE of Barcelona, Philippines	02 2023 14:48:41	8.3993, 126.7463
4	5.3	67 km ENE of Hinatuan, Philippines	02 2023 15:00:11	8.6266, 126.8901
5	5.8	65 km ENE of Barcelona, Philippines	02 2023 15:06:46	8.3198, 127.0017
6	5.4	25 km NE of Barcelona, Philippines	02 2023 15:08:56	8.3335, 126.5833
7	5.4	31 km NE of Barcelona, Philippines	02 2023 15:22:05	8.3389, 126.6551
8	5.5	48 km ENE of Hinatuan, Philippines	02 2023 15:31:29	8.4758, 126.7648
9	5.3	58 km ENE of Hinatuan, Philippines	02 2023 15:42:47	8.5072, 126.852
10	5.3	63 km ENE of Hinatuan, Philippines	02 2023 15:46:24	8.515, 126.8914
11	6.4	47 km NE of Barcelona, Philippines	02 2023 16:03:41	8.4377, 126.757
12	5.3	45 km ENE of Hinatuan, Philippines	02 2023 16:09:04	8.5779, 126.6901
13	5.6	46 km ENE of Hinatuan, Philippines	02 2023 16:17:01	8.4904, 126.7396
14	5.7	45 km ENE of Barcelona, Philippines	02 2023 16:19:46	8.3677, 126.7855
15	5.4	44 km NE of Hinatuan, Philippines	02 2023 16:34:59	8.6092, 126.6631
16	5.7	54 km ENE of Barcelona, Philippines	02 2023 16:53:08	8.4005, 126.8647
17	5.3	34 km NE of Barcelona, Philippines	02 2023 17:02:01	8.3663, 126.666
18	6.1	41 km NE of Barcelona, Philippines	02 2023 17:40:15	8.423, 126.722
19	5.6	21 km ENE of Hinatuan, Philippines	02 2023 17:42:16	8.4261, 126.5207
20	5.4	45 km ENE of Barcelona, Philippines	02 2023 17:43:14	8.2748, 126.8279
21	5.4	21 km NE of Barcelona, Philippines	02 2023 17:45:05	8.3044, 126.5663
22	5.6	52 km ESE of Marihatag, Philippines	02 2023 17:55:28	8.6642, 126.7521
23	6.3	63 km ENE of Barcelona, Philippines	02 2023 18:09:25	8.4402, 126.9387
24	5.4	37 km NE of Hinatuan, Philippines	02 2023 18:20:40	8.5944, 126.6118
25	5.3	59 km NE of Barcelona, Philippines	02 2023 19:17:00	8.4791, 126.8697
26	5.3	52 km ENE of Barcelona, Philippines	02 2023 19:19:21	8.4136, 126.8349
27	5.3	58 km NE of Barcelona, Philippines	02 2023 19:37:00	8.4696, 126.8694
28	5.4	36 km ENE of Barcelona, Philippines	02 2023 20:39:30	8.259, 126.7494
29	6	49 km NE of Barcelona, Philippines	02 2023 20:52:15	8.4475, 126.7782
30	5.5	55 km ENE of Barcelona, Philippines	02 2023 22:35:41	8.3688, 126.8873
31	5.3	60 km ENE of Hinatuan, Philippines	03 2023 02:02:37	8.5953, 126.8367
32	5.4	44 km ESE of Marihatag, Philippines	03 2023 05:43:43	8.6422, 126.6671
33	6.6	47 km ENE of Hinatuan, Philippines	03 2023 10:35:52	8.488, 126.7454
34	5.7	37 km ENE of Hinatuan, Philippines	03 2023 10:39:23	8.5597, 126.6174
35	5.5	69 km ENE of Barcelona, Philippines	03 2023 10:53:05	8.2897, 127.0525
36	5.6	61 km ENE of Hinatuan, Philippines	03 2023 10:54:55	8.5622, 126.862
37	5.4	57 km E of Aras-asan, Philippines	03 2023 10:58:38	8.8293, 126.83
38	5.4	81 km E of Marihatag, Philippines	03 2023 12:39:36	8.6744, 127.0239
39	6	58 km E of Marihatag, Philippines	03 2023 14:35:56	8.732, 126.823

keyboard blocks in the seismic source relative to their initial position. The full time of tsunami source generation takes 130 sec.

For the second scenario the of the earthquake source is located along the subduction zone.

Figure 6 shows a schematic representation of the source for Scenario 2. The seismic source dimensions were estimated using the Wells formulae [*NOAA*, 2023].

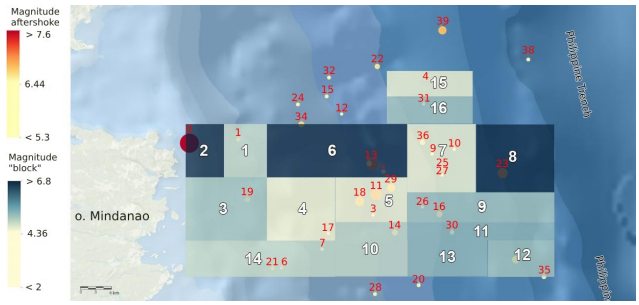

Figure 5. Visualization of the constructed earthquake source for the first scenario, where the big red point is corresponds to the epicenter of the earthquake; orange and yellow circles correspond to aftershocks of the earthquake.

Table 2. Data for realization of earthquake source dynamics (Scenario 1)

Block number	X1	Y1	X2	Y2	Start time	Movement time	Displacement value
1	126.478	8.560	126.410	8.465	0	20	6
2	126.556	8.560	126.478	8.465	0	20	3.5
3	127.070	8.386	126.807	8.354	0	20	4
4	126.556	8.465	126.931	8.439	0	20	3
5	126.556	8.465	126.410	8.353	20	10	3.8
6	126.410	8.289	126.677	8.289	30	15	3.5
7	126.931	8.439	127.070	8.559	45	15	6
8	126.807	8.560	126.930	8.439	60	10	3
9	126.678	8.465	126.678	8.386	60	10	3
10	126.807	8.386	126.677	8.290	30	15	3.5
11	126.556	8.560	126.556	8.465	70	20	5
12	126.807	8.439	127.070	8.386	90	15	3.8
13	126.770	8.609	126.924	8.653	105	10	3
14	126.556	8.560	126.679	8.635	115	15	4
15	127.070	8.354	126.952	8.289	90	15	3.8
16	126.770	8.560	126.924	8.609	130	15	3.8

For this case, a source consisting of 18 blocks is considered (Figure 7). The characteristics of block motion differ significantly from the data given in the first scenario (Table 3). It can be seen that for the second scenario the movement of each block occurs in two stages, taking into account the time of occurrence of the aftershock, the localization of which coincides with this block. The process of tsunami source generation at such motion of keyboard blocks in the earthquake source takes 310 sec and has rather complicated initial structure of formation (Figure 7).

3. Numerical simulation of the spatial and temporal characteristics of tsunami wave propagation over the computed water area

To describe the modeling of tsunami generation and propagation, the paper applies a system of nonlinear shallow water equations, which can be represented in the following form [see, e.g., eq. *Lobkovsky et al.*, 2006; *Pelinovsky and Mazova*, 1992; *Stocker*, 1957; *Voltsinger et al.*, 1989]:

$$\begin{cases} \vec{U}_t + \vec{U} \cdot \operatorname{grad} \vec{U} + g \cdot \operatorname{grad} \eta = \vec{F}, \\ \eta_t + \operatorname{div}\left((H + \eta - B)\vec{U}\right) = B_t, \end{cases}$$

Table 3. Data for realization of earthquake source dynamics (Scenario 2)

Blocks number	1	2	3	4	5	6	7	8	9	10	11	12	13	14	15	16	17	18
M magnitude		5.4	6	5.7	5.2		7.6	5.4		5.5	5.3	5.3	5.3	5.7	5.4	5.4	5.4	
Start of a movement, s		270	280	130	40		0	10		100	40	100	70	160	70	10	180	
Heights, m		2.4	3.0	2.8	2.2		8	2.4		2.5	2.3	2.3	2.3	2.8	2.4	2.4	2.4	
Movement time, s		10	30	30	30		10	30		20	30	20	30	20	30	30	20	
End of movement time, s		280	310	160	70		10	40		120	70	120	100	180	100	40	200	
Blocks number	1	2	3	4	5	6	7	8	9	10	11	12	13	14	15	16	17	18
M magnitude				5.3	5.6					6.6	6.1	5.3	5.3		5.3		5.6	
Start of a movement, s				210	180					270	120	240	200		200		240	
Heights, m				2.3	2.6					3.5	3.1	2.3	2.3		2.3		2.6	
Movement time, s				30	10					10	10	30	10		10		30	
End of movement time, s				240	200					280	130	270	210		210		270	

where η is the water surface displacement, H is the basin depth, function $B(x,y,t)$ describes the displacement of the bottom surface relative to the initial position; g is the gravity acceleration; $\overset{r}{U} = \begin{pmatrix} u \\ v \end{pmatrix}$, $u(x,y,t)$, $v(x,y,t)$ are depth-averaged horizontal components of the wave velocity. The Coriolis force and the friction force, represented by the function $\overset{r}{F}$:

$$\overset{r}{F} = \begin{pmatrix} fv - g\dfrac{u\sqrt{u^2+v^2}}{C_h^2(H+\eta-B)} \\ -fu - g\dfrac{v\sqrt{u^2+v^2}}{C_h^2(H+\eta-B)} \end{pmatrix}.$$

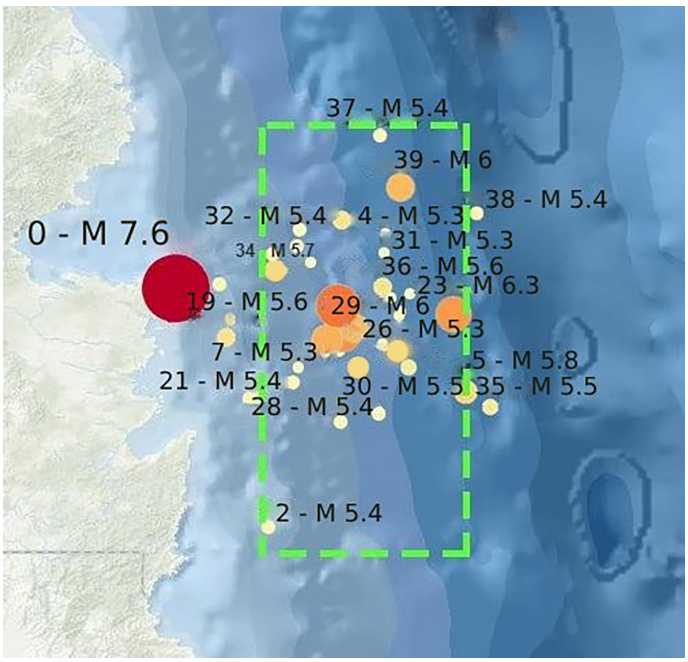

Figure 6. Schematic localization of earthquake source in Philippines 02.12.2023 colored circles correspond to aftershocks, with marked on them aftershock magnitudes and sequence of aftershock occurrence.

The Shezi coefficient was found using the formula:

$$C_h = \frac{(H + \eta - B)^{0.4}}{S_h},$$

where S_h is the roughness coefficient, $f = 2\Omega \cos\theta$ is the Coriolis parameter, Ω is the angular velocity of the Earth, θ is the geographic latitude of the Earth. Sphericity of the Earth is not taken into account. For modeling, we used the bathymetry of the Philippine Sea, the spatial step was approximately 900 m (30”).

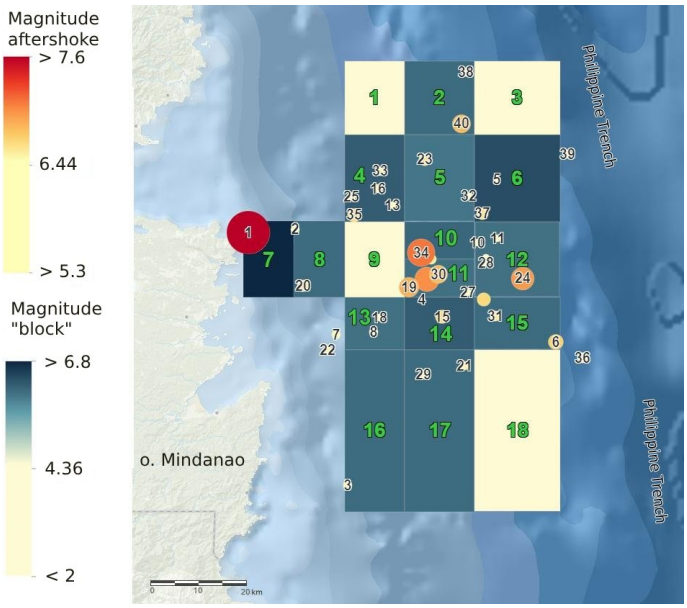

Figure 7. Visualization of the constructed earthquake source for the second scenario, where the big red point corresponds to epicenter of the earthquake; orange and yellow circles correspond to aftershocks of the earthquake.

Figure 8 shows 8 time moments during the generation of a tsunami source for Scenario 1 (Table 2). Figure 9 shows 4 time moments during the propagation of tsunami waves across the computed water area for Scenario 1.

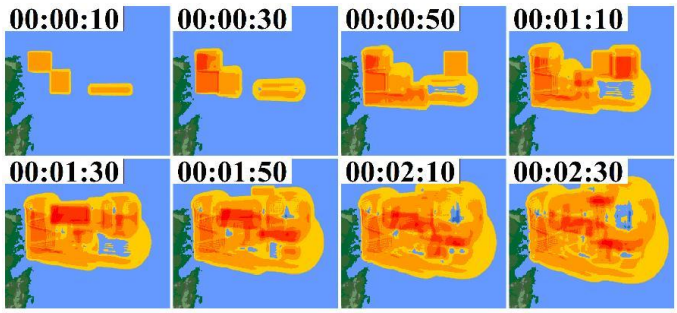

Figure 8. Generation of a tsunami source by a seismic source shown in Figure 4.

Figure 10 shows the generation of a tsunami source during the implementation of Scenario 2 for 8 time moments. The process of tsunami wave propagation during the implementation of Scenario 2 is shown in Figure 11.

As in the first scenario, the waves propagate in concentric circles from the source, reflecting from underwater obstacles and forming complex interference patterns. It is clearly seen (Figures 9 and 11) that when propagating across the water area, the waves interact with underwater obstacles and islands along their path. This leads to the phenomena of reflection, diffraction and refraction of waves, forming complex interference

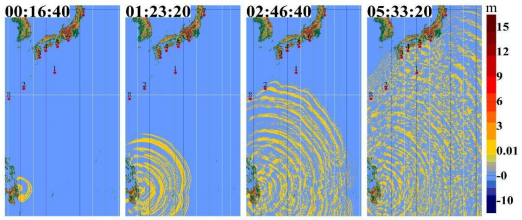

Figure 9. Propagation of wave fronts across the Philippine Sea from the island of Mindanao (Philippines) to the Japanese Islands for 4 time moments during the implementation of Scenario 1.

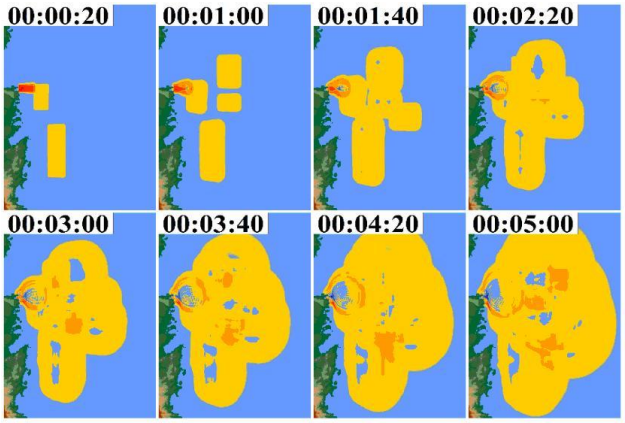

Figure 10. Generation of a tsunami source by a seismic source shown in Figure 4.

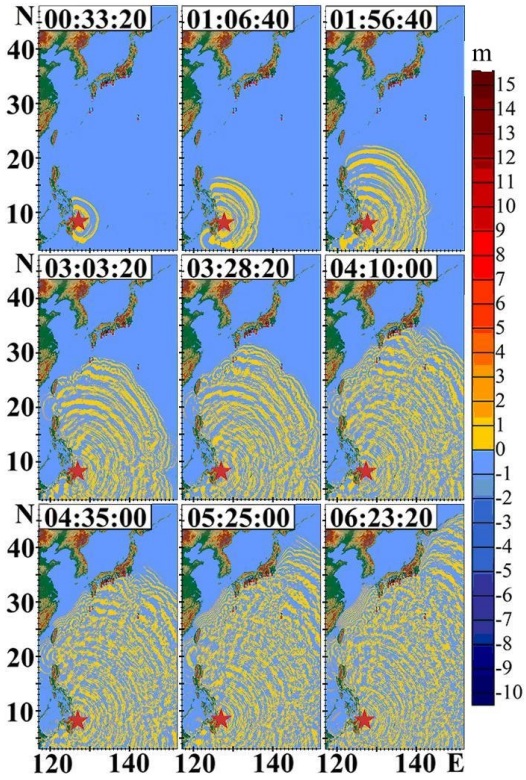

Figure 11. Propagation of wave fronts across the Philippine Sea from the island of Mindanao (Philippines) to the Japanese Islands for 9 time moments during the implementation of Scenario 2. (the asterisk indicates the epicenter of the earthquake, the color shows the wave height at each point).

patterns. As tsunami waves propagate, they gradually lose their energy due to dissipation and interaction with the submarine relief. It can be seen that the waves first reach the

coast of the Kimotsuki area in Kagoshima Prefecture approximately 3.5 hours after the earthquake. After about another 30 minutes, the waves reach the island of Shikoku, and 6 hours after the start of the simulation, the waves cover the entire southeastern coast of the Japanese islands. It should be noted that despite significant differences in the location of the source and parameters of wave generation, the general nature of their propagation remains to be similar for the two considered scenarios.

In Figures 12 and 13 it can be seen the distribution of maximum wave heights throughout the entire computed water area. It can be also seen that the areas with the highest wave heights, shown in purple, are concentrated near the source, and as they move away from the source, the wave heights become lower.

It is clearly seen that for Scenario 2, near the earthquake source, the wave heights are larger compared to the waves from the first source. However, as we move away from the sources, the difference in maximum wave heights between the two scenarios gradually smoothes out and the wave heights from both sources reach comparable maximum values. In Figure 14 and Figure 15 2D histograms are presented for the distribution of tsunami wave heights on a 5-meter isobath along the coast of the Japanese Islands, where data obtained after the first scenario is shown in red, and data obtained after the second scenario is shown in blue.

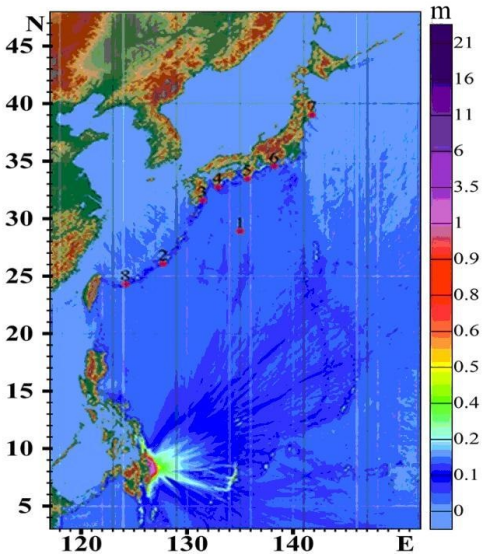

Figure 12. Distribution of maximum wave heights for the first scenario over the Pacific Ocean of from the Philippine Islands to the Japanese Islands.

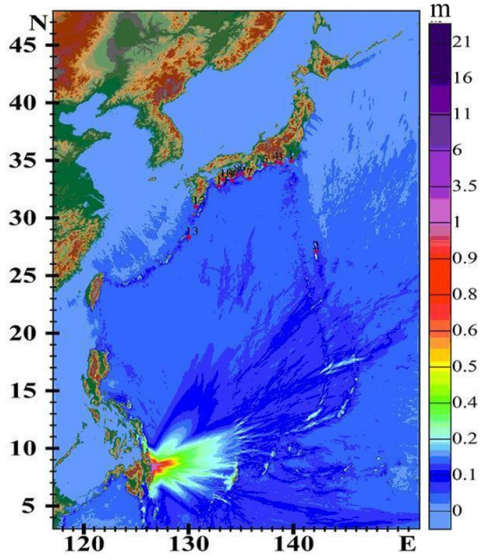

Figure 13. Distribution of maximum wave heights for the second scenario over the Pacific Ocean of from the Philippine Islands to the Japanese Islands.

Based on the above figures, it can be concluded that in both scenarios considered, the highest maximum wave heights were observed in two regions of Japan. The first region covers the part of Honshu Island located between 135° and 138°E, where the waves reached their maximum values. The second region, where significant maximum wave heights were also observed, is located on Shikoku Island in the longitude range from 133° to 134.8°E. Thus, despite the differences in scenarios, these two zones along the Japanese islands experienced the greatest impact of tsunami waves. Figures 16 and 17 present 3D histograms showing the maximum wave heights along the coast of Japan at the 5-meter isobath, along the southeastern coast of Kyushu and Honshu Island (Figure 16) and along the southeastern coast of Shikoku Island (Figure 17).

Figures 19, 20 show 3D histograms showing the maximum wave heights along the coasts of the People's Republic of China and the Republic of Korea.

It is clearly seen that during this earthquake, wave heights along the coasts of these countries do not exceed 60 cm for the coast of China, and 10 cm for the Republic of Korea.

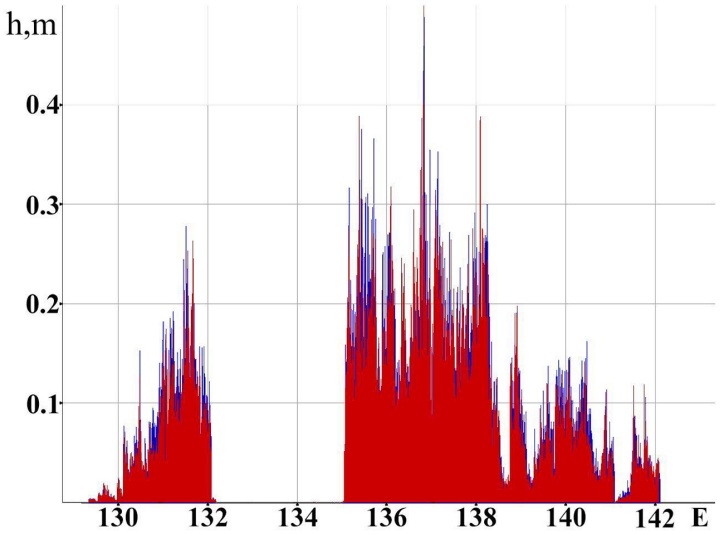

Figure 14. 2D histogram of the distribution of maximum wave heights along the southeastern coast of Kyushu Island (from 129°E to 132°E) and Honshu Island.(from 135°E to 142°E).

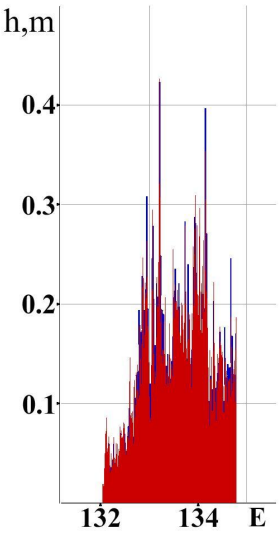

Figure 15. 2D histogram of the distribution of maximum wave heights along the southeastern coast of Shikoku Island (from 132°E to 134.8°E).

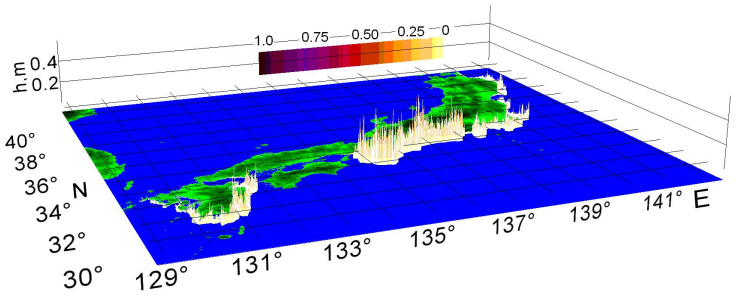

Figure 16. 3D histogram of the distribution of maximum wave heights along the southeastern coast of Kyushu Island (from 129°E to 132°E) and Honshu Island (from 135°E to 142°E). Scenario 1.

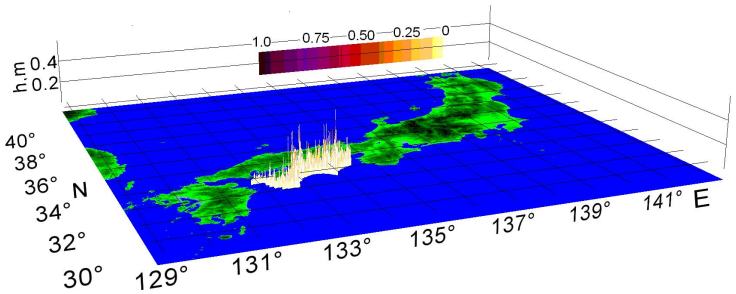

Figure 17. 3D histogram of the distribution of maximum wave heights along the southeastern coast of Shikoku Island (from 132°E to 134.8°E). Scenario 1.

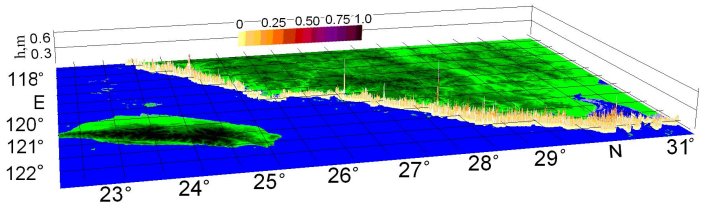

Figure 18. 3D histogram for the Yellow Sea coast from Fujian to Shanghai. Scenario 1.

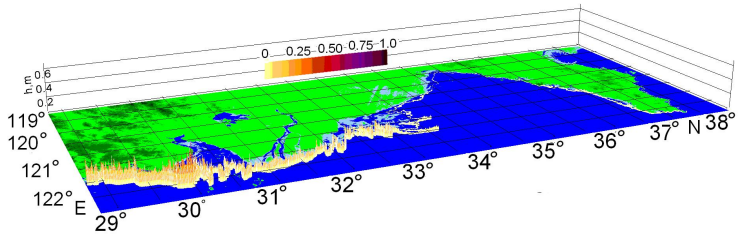

Figure 19. 3D histogram for the Yellow Sea coast from Fujian to Qingdao. Scenario 1.

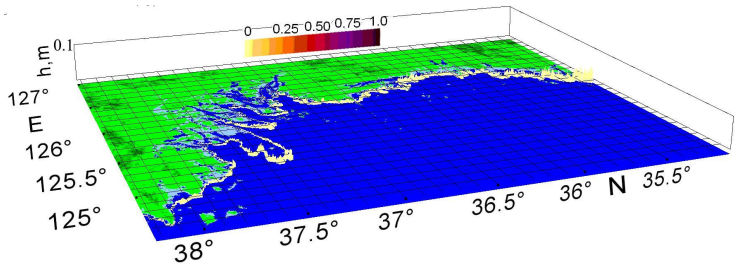

Figure 20. 3D histogram for the coast of the Republic of Korea. Scenario 1.

4. Comparison of simulation results with observational data

To compare the results of numerical simulation of tsunami waves and assess the accuracy of the methods used, a comparison was made with data obtained from real observations. A comparison was made for the maximum tsunami wave heights obtained by virtual tide gauges in the in the program complex and records by real observation stations. The obtained data are presented in Table 4.

Table 4. Comparison of observed data and numerical simulations data of two scenarios at the locations of virtual tide gauges

No.	Name of items with localization of tide gauges	Maximum displacement, cm		
		Tide gauge data [*NOAA*, 2024; *UNESCO*, 2024; *USGS*, 2024]	Numerical calculation	
			Scenario 1	Scenario 2
1	MERA (139.82, 34.91)	10	12.4	10.4
2	CHICHIJIMA ISLAND (142.19, 27.09)	5	33.4	32.8
3	TAGO (138.76, 34.8)	5	13.6	15.3
4	YAIZU (138.33, 34.86)	5	4.1	2.5
5	TAHARA (137.27, 34.66)	5	16.9	16.4
6	GOBO (135.16, 33.85)	10	27.3	29.9
7	KUSHIMOTO (135.78, 33.46)	10	10.2	20
8	YUKI (134.6, 33.76)	5	15.5	17.5
9	MUROTOMISAKI (134.16, 33.26)	5	22.2	25.1
10	KURE (133.25, 33.33)	5	18.2	13.8
11	TOSA-SHIMIZU (132.95, 32.77)	10	21.5	23.4
12	ODOMARI (130.68, 31.01)	10	4.2	15.3
13	KOMINATO, AMAMI ISLAND (129.53, 28.31)	10	5.4	6.7

The data presented in Table 4 can also be seen in the comparison graph (Figure 21).

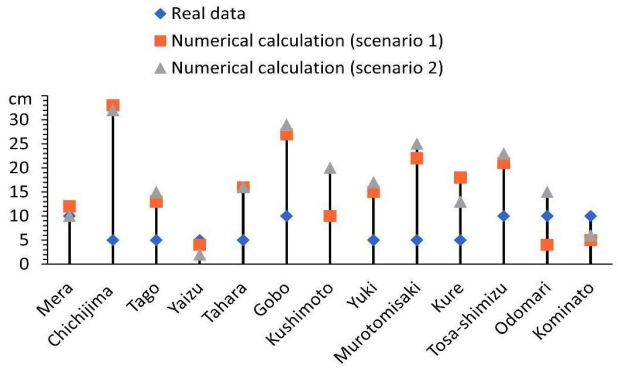

Figure 21. Graphic comparison of the results of computation of tsunami wave heights at a number of points in the computed water area.

5. Conclusions

In the paper a strong earthquake off the coast of the island of Mindanao, in the Philippines, which occurred on December 23, 2023 with a magnitude of $M = 7.6$ is studied. Possible model seismic sources of this earthquake were constructed, and the possible kinematics of keyboard blocks in the earthquake source were analyzed. Numerical simulation of the generation and propagation of tsunami waves was carried out for two earthquake scenarios. Maximum wave heights and time to reach several coastal locations were estimated for both scenarios. The highest wave heights were obtained in the southeastern part of the island of Honshu, located between 135° and 138°E, as well as the southeastern part of the island of Shikoku in the longitude range from 133° to 134.8°E. Comparative assessments of data from virtual tide gauges using numerical simulation and available field data from tide gauge stations were made. As can be seen from the Table, 4 a good agreement was obtained for maximum wave heights in a number of mainland and island locations. Thus, numerical simulation of a seismic tsunami using a keyboard model of a seismic source made it possible to obtain important information about the characteristics of the generated waves, their propagation and impact on coastal areas.

Acknowledgments. This work was supported by the Laboratory of Nonlinear Hydrophysics and Natural Disasters of the V.I. Il'ichev Pacific Oceanological Institute, grant of the Ministry of Science and Higher Education of the Russian Federation (agreement No. 075-15-2022-1127 dated July 1, 2022).

References

Lobkovsky, L. I., and B. V. Baranov (1984), Keyboard model of strong earthquakes in island arcs and active continental margins, *Doklady Akademii Nauk SSSR*, *275*(4), 843–857 (in Russian).

Lobkovsky, L. I., B. V. Baranov, R. K. Mazova, and L. Y. Kataeva (2006), Implications of the seismic source dynamics for the characteristics of a possible tsunami in a model problem of the seismic gap in the Central Kurile region, *Russian Journal of Earth Sciences*, *8*(5), https://doi.org/10.2205/2006ES000209.

NOAA (2023), M 7.6 - 19 km E of Gamut, Philippines, https://www.ngdc.noaa.gov/hazel/view/hazards/earthquake/event-more-info/10721, (visited on 24/08/10).

NOAA (2024), Latest news and features, http://earthquake.usgs.gov, (visited on 24/08/10).

Pelinovsky, E. N., and R. K. Mazova (1992), Exact analytical solutions of nonlinear problems of tsunami wave run-up on slopes with different profiles, *Natural Hazards*, *6*(3), 227–249, https://doi.org/10.1007/BF00129510.

Stocker, J. J. (1957), *Water Waves The Mathematical Theory With Applications*, Interscience Publishers, New York.

UNESCO (2024), International Tsunami Information Centre, http://www.tsunamiwave.info/, (visited on 24/08/10).

USGS (2023), Significant Earthquake Information, https://earthquake.usgs.gov/earthquakes/eventpage/us7000lff4/executive, (visited on 24/08/10).

USGS (2024), Significant Earthquakes - 2024, http://earthquake.usgs.gov, (visited on 24/08/10).

Voltsinger, N. E., K. A. Klevanniy, and E. H. Pelinovskiy (1989), *Long-Wave Dynamics of Coastal Zone*, 271 pp., Gidrometeoizdat, Leningrad (in Russian).

Wells, D. L., and K. J. Coppersmith (1994), New empirical relationships among magnitude, rupture length, rupture width, rupture area, and surface displacement, *Bulletin of the Seismological Society of America*, *84*(4), 974–1002, https://doi.org/10.1785/BSSA0840040974.

Wikipedia (2024a), December 2023 Mindanao earthquake, https://en.wikipedia.org/wiki/December_2023_Mindanao_earthquake, (visited on 24/08/10).

Wikipedia (2024b), Data:December 2023 Mindanao earthquake.map, https://commons.wikimedia.org/wiki/Data:December_2023_Mindanao_earthquake.map, (visited on 24/08/10).